Desalination and Water Treatment
www.deswater.com

doi: 10.5004/dwt.2019.23606

146 (2019) 245–256
April

Cadmium removal from aqueous solution by iron oxide coated sepiolite: preparation, characterization and batch adsorption studies

İlker Kıpçak*, Ceren Akın

Department of Chemical Engineering, Eskişehir Osmangazi University, Eskişehir 26480, Turkey, Tel. +90(222)2393750; Fax: +90(222)2290535; emails: ikipcak@ogu.edu.tr (İ. Kıpçak), cerengurakan@gmail.com (C. Akın)

Received 4 September 2018; Accepted 13 December 2018

ABSTRACT

In this study, iron oxide coated sepiolite (IOCS) as a new composite adsorbent was synthesized and employed for the removal of Cd(II) ions from aqueous solutions by adsorption. The synthesized composite was characterized by X-ray diffractogram, X-ray fluorescence, BET, scanning electron microscopy, energy dispersive spectroscopy and Fourier transform infrared spectroscopy analyses. Batch adsorption experiments were conducted to investigate the effects of adsorbent dosage, pH, contact time, initial concentration and temperature on the cadmium ions uptake. The kinetics of adsorption has been studied, and various kinetic models, such as pseudo-first-order, pseudo-second-order and intraparticle diffusion models were tested with experimental data for their validity. The pseudo-second-order kinetic model was determined to correlate well to the experimental data. The Langmuir and Freundlich isotherms were utilized for the analysis of adsorption equilibrium. The Langmuir isotherm gave a better fit for Cd(II) adsorption and the maximum loading capacity was found as 98.04 mg g^{-1} at 25°C. This value was almost three times bigger than that of raw sepiolite. The calculated thermodynamic parameters showed that the adsorption of Cd(II) ions is feasible, spontaneous and endothermic in nature. Experimental results indicated that the IOCS appear to be a promising adsorbent material for the removal of cadmium ions from aqueous media.

Keywords: Adsorption; Cadmium removal; Iron oxide coating; Sepiolite

1. Introduction

Heavy metals are generally recognized as a threat towards human health and ecosystems because of their high persistence in surface and ground water [1]. The metals hazardous to human include arsenic, mercury, chromium, lead, nickel, cadmium, cobalt and copper [2]. Among these, cadmium is recognized as one of the most harmful heavy metal pollutants in the environment due to its toxicity, non-degradability, bioaccumulation and mobility in natural water and soil ecosystems. It is highly carcinogenic and may cause endocrine disorders as well as renal dysfunction and bone fracture [3]. The World Health Organization has set a maximum guideline concentration of 0.003 mg L^{-1} for cadmium in drinking water [4]. Therefore, it is very essential to control the concentration of heavy metals in wastewater before its disposal into the environment. There are many chemical and physical processes to remove heavy metals from water. Classical techniques used for remediation and clean-up of heavy metal ions from polluted environment include precipitation, coagulation, ultrafiltration, reverse osmosis, electrodialysis, ion exchange and adsorption [3]. Among these methods, adsorption is one of the promising technologies due to its high removal efficiency and simplicity, provided easy availability of low-cost adsorbents that can be found locally [5]. It was also reported that, in case of low-cost adsorbents, the modification of the adsorbent increases the removal efficiency [6].

Nanometer iron, its oxides and hydroxides are promising adsorbents for the removal of metal ions from water due to their strong affinity for metal species, leading to a high adsorption

* Corresponding author.

capacity. The ease of the fabrication of these nanoparticles also makes them popular applicants in metal removal [7]. However, most of these iron species are only available as fine powder and their usage is limited because of the difficulty in separation of the solid from the solution. Therefore, some substrates with high surface area such as activated carbon, biomass, sand, silica and clays were used to support iron oxide nanoparticles to increase their dispersion and mechanical properties. The adsorption capacity seems to depend on the surface properties of the coated materials which could be related to the nature of the supporting materials [8].

Sepiolite, also known as meerschaum, is a natural hydrated magnesium silicate clay mineral. The mineral contains zeolitic water in intracrystalline tunnels and has an idealized half unit cell formula $Si_{12}O_{30}Mg_8(OH)_4(OH_2)_4{\cdot}8H_2O$, where ($OH_2$) represents crystal water and H_2O zeolitic water. Structurally, it is formed by blocks and channels extending in the fibre direction (c axis). Each structural block is composed of two tetrahedral silica sheets and a central octahedral sheet containing magnesium. Due to the discontinuity of the external silica sheet, a significant number of silanol (Si–OH) groups are present at the surface of this mineral [9–11]. Several deposits of sepiolite have been reported in Turkey and the most commercially used sepiolite is mined from Eskişehir province. Türkmentokat-Gökceoğlu region is the most important and high-quality meerschaum producing district in Eskişehir. Sepiolite is mostly used to make souvenirs, especially tobacco pipes (known as meerschaum pipes) by carving. Recently, sepiolite has been examined by many researchers for use as a sorbent material [12–14]. The mineral has a unique structure, composition, porosity and high surface area. So this mineral should provide an efficient surface for the iron oxides. At the same time, the iron oxides can improve the heavy metal adsorption capacity of sepiolite [12]. Therefore, the combination of sepiolite and iron oxides seems as a promising adsorbent material to remove heavy metals from aqueous media. To our knowledge, whereas, no study has explored the performance of iron oxide coated sepiolite (IOCS) on the removal of cadmium although the adsorption behaviour of IOCS for lead, copper and nickel were examined by some researchers [12–14].

For these reasons, the aim of this study is to examine the effectiveness of IOCS in the removal of Cd(II) ions from aqueous solutions and to determine the adsorption characteristics. The effects of various experimental parameters such as adsorbent dosage, pH, contact time, initial concentration and temperature have been studied. Adsorption isotherms, kinetics and thermodynamic parameters were also evaluated.

2. Materials and methods

2.1. Materials

The natural sepiolite used in this study was supplied from a workshop as carving residue and excavated from Türkmentokat-Gökçeoğlu region in Eskişehir, Turkey. It was ground and sieved under 75 μm using an ASTM standard sieve, and then dried at 105°C for 3 h. All chemicals used in the experiments were purchased as of analytical purity and all solutions were prepared with distilled water. A stock solution containing 1,000 mg L^{-1} of Cd(II) was prepared by dissolving a predetermined amount of $3CdSO_4{\cdot}8H_2O$ in distilled water. The stock was diluted to prepare desired working solutions.

2.2. Preparation of iron oxide coated sepiolite

A 20 g sample of sepiolite was immersed in 200 mL of freshly prepared 0.5 M $Fe(NO_3)_3{\cdot}9H_2O$ solution in a glass beaker. The mixture was stirred with a magnetic stirrer at the rate of 500 rpm for 4 h. Then 400 mL of 1.0 M NaOH aqueous solution was added dropwise to precipitate the iron oxide on the surface of sepiolite. The beaker was covered with a stretch film and the suspension was stirred for 48 h at 60°C. Then the cover on the beaker was opened and the mixture was heated to dryness. The solid sample was ground and washed several times with distilled water to remove unattached oxides. The particular sample was dried at 105°C for 24 h and finally stored in a capped bottle for further use. The raw sepiolite and the iron oxide coated sepiolite samples were denoted as RS and IOCS, respectively.

2.3. Characterization methods

The chemical analyses of RS and IOCS were performed by a ZSX Primus model X-ray fluorescence (XRF; Rigaku) analyser. Their X-ray diffractograms (XRDs) were obtained with a Rigaku RINT 2000 model diffractometer. The BET specific surface areas and porous properties of RS and IOCS samples were determined from N_2 adsorption experiments using a Quantachrome Autosorb 1C analyser. The samples were degassed for 3 h at 573 K to remove any moisture or adsorbed contaminants that may have been present on their surfaces. The scanning electron micrographs were obtained using JSM 5600LV (JEOL) scanning electron microscope (SEM). The energy dispersive spectroscopy (EDS) analysis was performed by using IXRF Systems 550i. Fourier transform infrared spectroscopy (FTIR) spectra of the samples were recorded using KBr pellets on Spectrum 100 model infrared spectrophotometer (PerkinElmer) over 400–4,000 cm^{-1}.

2.4. Adsorption studies

Batch adsorption experiments were carried out by varying adsorbent dosage, initial solution pH, contact time, initial concentration and temperature. A fixed amount of the adsorbent and 50 mL of Cd(II) solution were placed in a capped volumetric flask and shaken at 150 rpm using a temperature-controlled water bath with shaker for determined time intervals at constant temperatures. After adsorption, the adsorbent was filtered from a blue ribbon filter paper and the Cd(II) concentration retained in the solution was determined by Thermo ICE 3300 model atomic absorption spectrophotometer at 228.8 nm wavelength. The percentage of Cd(II) removal was then calculated using the following equation:

$$\text{Removal}\ (\%) = \left(\frac{c_0 - c_t}{c_0}\right)100 \tag{1}$$

where C_0 and C_t are the concentrations in the solution (mg/L) at time t = 0 and at time t (min), respectively. From the mass

balance, the amount of Cd(II) adsorbed per unit mass of IOCS (q, mg/g) was calculated using the following equation:

$$q = (c_0 - c_t)\frac{v}{m} \quad (2)$$

where V is the volume of the treated solution (L) and m is the mass of adsorbent (g).

Different adsorbent dosages (0.01–0.20 g/50 mL) were applied to investigate the effect of adsorbent dosage on the removal of Cd(II) ions. The effect of solution pH was investigated by varying the initial solution pH from 2 to 6. The pH was adjusted by addition of 0.1 M HCl or 0.1 M NaOH into the solution. The pH value was measured by a pH meter (HI 8314, Hanna, Portugal). Batch experiments were also repeated for various time intervals (5–1,440 min) to determine the time required to reach equilibrium. The adsorption isotherms were obtained by varying the initial Cd(II) concentration from 50 to 500 mg L^{-1} at three different temperatures (25°C, 35°C and 45°C).

3. Results and discussion

3.1. Characterization results

The chemical compositions of RS and IOCS determined by XRF analyses are given in Table 1. It can be seen from the table that the Fe_2O_3 content of RS increased from 0.24% to 29.58% for the coated mineral. The XRD results of RS and IOCS samples are given in Fig. 1. The XRD spectra of RS showed the characteristic diffraction reflections of sepiolite (Fig 1(a)). It mainly composed of sepiolite and small amounts of magnesite ($MgCO_3$) and dolomite ($CaMg(CO_3)_2$). The main reflection was observed in 5° < 2θ < 9° region. This corresponds to the 7.11 (2θ) value from which the interlamellar distance was found to be 12.43 Å. The XRD results showed that the iron oxide coating process caused structural changes in the sepiolite sample. After the iron oxide coating process, the intensity of the 110 reflection has been reduced and its position shifted from 7.11 to 7.21 [13]. It can be understood from the XRD of IOCS that the magnesite and dolomite ingredients were removed during the preparation of the composite (Fig. 1(b)). The increase in the SiO_2:MgO ratio during modification also confirmed this result (Table 1). The decrease in the loss on ignition (LOI) value after coating was another indicator of the removal of carbonate compounds and also water. The new peak observed in the XRD spectra of IOCS indicated the formation of maghemite (γ-Fe_2O_3) or magnetite (Fe_3O_4) on IOCS. Thus, the XRD analysis of the composite confirmed the occurrence of Fe-oxidized phase [15,16].

Table 1
Chemical compositions of RS and IOCS

Component (%, w/w)	RS	IOCS
MgO	30.73	20.92
SiO_2	48.91	34.95
CaO	2.38	1.57
Fe_2O_3	0.24	29.58
LOI	17.73	12.97

The data in Table 2 indicate the surface areas, pore volumes and average pore diameters for the RS and IOCS samples. The BET specific surface area increased from 182.19 $m^2 g^{-1}$ for RS to 220.70 $m^2 g^{-1}$ for the composite material. This could be explained by the presence of magnetic iron oxide particles on the IOCS surface. In addition, the mesopore volume increased, but the micropore volume decreased after the coating treatment. This means that the micropores on sepiolite were occupied by iron oxides and some additional mesopores were formed.

The SEM and EDS spectra of the RS and IOCS samples are given in Fig. 2. The RS sample showed porous and fibrous morphology (Fig. 2(a)). There were scattered acicular minerals and mineral aggregates on its surface. Among them, the light coloured particles were magnesite or calcite impurities. Rough particles adhering onto the surface of IOCS indicated the iron oxide coating (Fig. 2(b)). The EDS analysis showed that the RS was composed mainly of Si and Mg and smaller amounts of Ca and Fe (Fig. 2(c)). The percentage of iron increased considerably after the iron oxide coating treatment (Fig. 2(d)). This shows that the coating was achieved successfully.

The FTIR spectra of the RS, IOCS and cadmium adsorbed IOCS (IOCS-Cd) samples are shown in Fig. 3. The possible functional groups for each sample are presented in Table 3. In the spectrum of RS, the IR band at 3,691 cm^{-1} was assigned

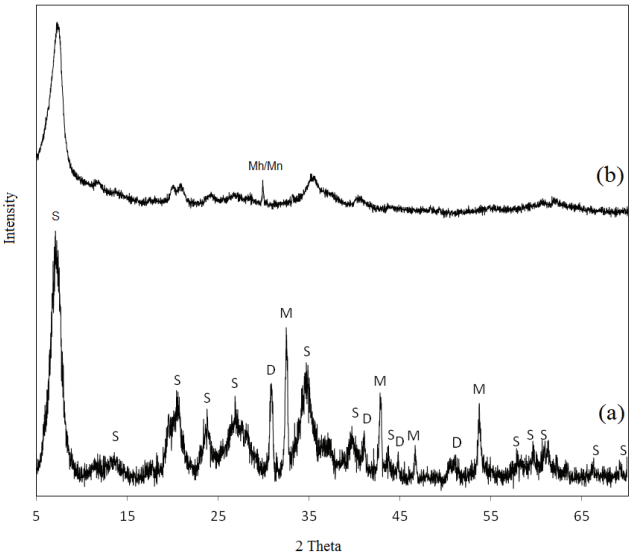

Fig. 1. XRD patterns of RS (a) and IOCS (b) samples (S: sepiolite, M: magnesite, D: dolomite, Mh: maghemite, Mn: magnetite).

Table 2
Textural properties deduced from N_2 adsorption at 77 K for the RS and IOCS

Sample	RS	IOCS
S_{BET} ($m^2 g^{-1}$)	182.19	220.70
V_{total} ($cm^3 g^{-1}$)	0.2160	0.2844
V_{micro} ($cm^3 g^{-1}$)	0.0054	0.0000
V_{meso} ($cm^3 g^{-1}$)	0.2106	0.2844
D_p (Å)	47.59	51.55

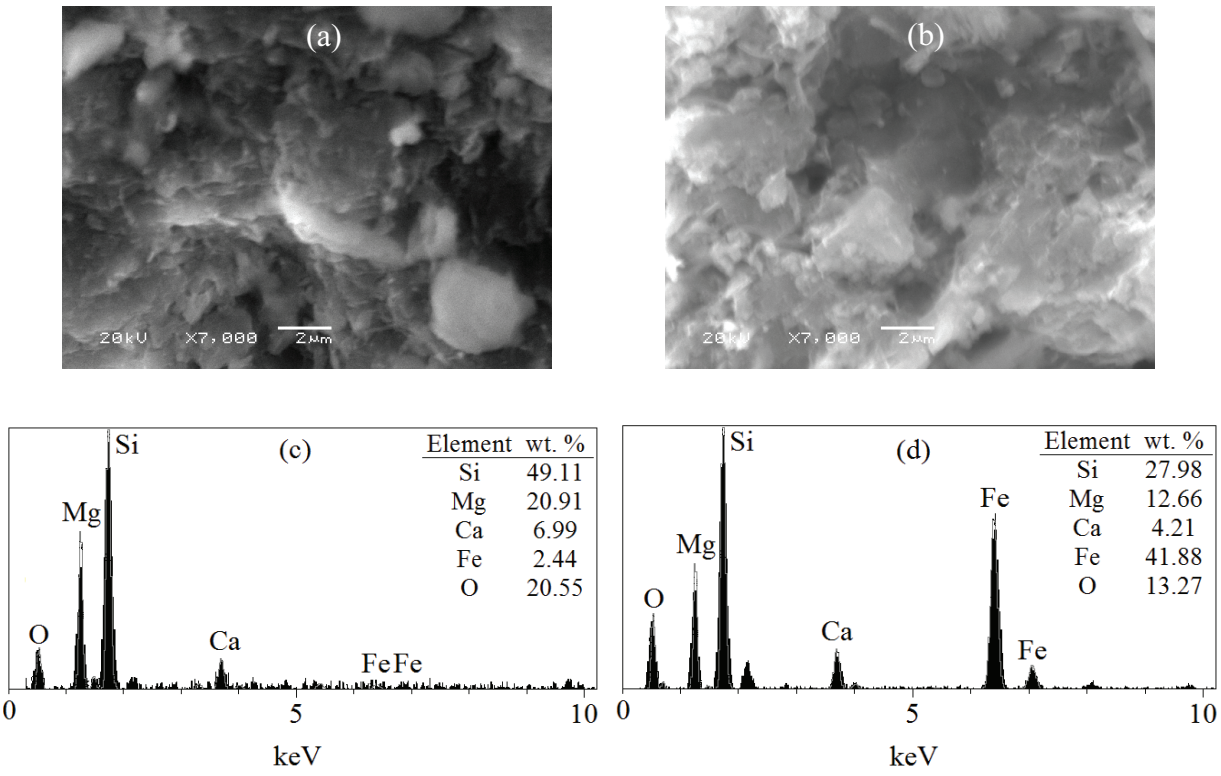

Fig. 2. SEM of RS (a) and IOCS (b); EDS of RS (c) and IOCS (d).

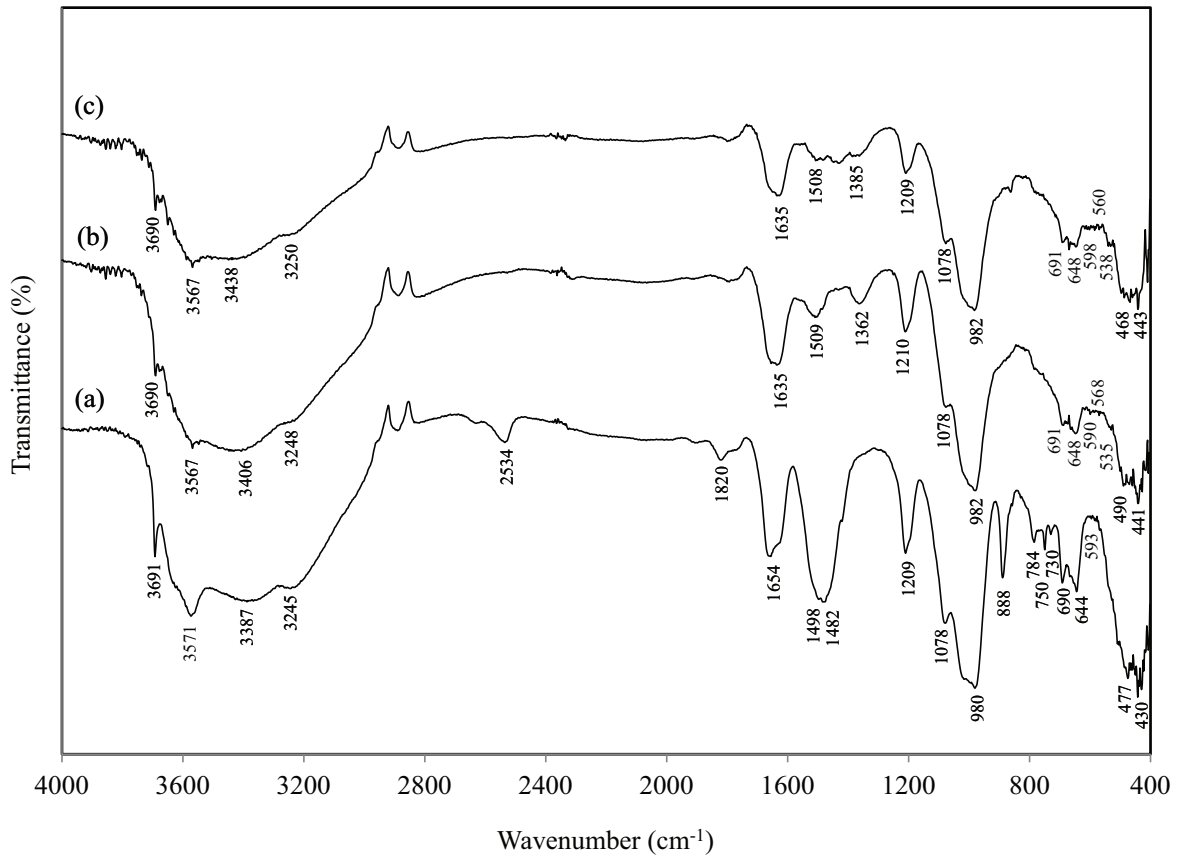

Fig. 3. FTIR spectra of RS (a), IOCS (b) and IOCS-Cd (c).

to the surface Mg-OH stretching vibration [12,17]. The band at 3,571 cm^{-1} was related with the stretching modes of molecular water coordinated with magnesium, and two bands at 3,387 and 3,245 cm^{-1} were attributed to zeolitic and coordinated waters, respectively [14,17,18]. The presence of dolomite and magnesite impurities was confirmed by the bands at 2,534; 1,820; 1,498; 1,482; 888 and 730 cm^{-1} [19–22]. The band at 1,654 cm^{-1} was due to the vibration of zeolitic water [21,23]. The bands in the 1,250–400 cm^{-1} range were characteristic of silicate structure of sepiolite. The bands observed at 1,209; 1,078 and 980 cm^{-1} were produced by the Si–O vibrations [13,24]. The band observed at 784 cm^{-1} was O–H bending vibration of Mg–Fe–OH [25]. The band at 750 cm^{-1} was assigned to the Si–O bonds [26]. The band at 477 cm^{-1} could be attributed to an O–Si–O bending [13,19]. The band at 430 cm^{-1} was originated from octahedral-tetrahedral bonds (Si–O–Mg bonds) and the bands at 690 and 644 cm^{-1} were corresponded to the Mg–OH bond vibrations [14,24]. The peak at 593 cm^{-1} could be assigned to the Fe–O stretching vibration [14].

As the RS altered to IOCS, noticeable changes in the IR absorption bands were detected (Fig. 3(b)). The intensities of the bands at 3,691 and 3,571 cm^{-1} decreased after iron oxide coating process. This result indicated the replacement of iron oxide particles with Mg^{2+} cations located at the edges of the octahedral layers. So, the water and hydroxyl groups coordinated to the Mg^{2+} cations were also removed. The decreasing intensity of the hydroxyl vibration of the zeolitic water (3,387 cm^{-1}) indicated the replacement of iron oxide particles with part of the zeolitic water. The shift of the band at 1,654 to 1,635 cm^{-1} indicated the decrease of the H_2O content with the replacement of iron oxide molecules [12]. For IOCS, the bands attributed to carbonate impurities (2,534; 1,820; 1,498; 1,482; 888 and 730 cm^{-1}) disappeared or shifted after the coating treatment, suggesting that these impurities were removed during coating (Table 3). These results were in good agreement with the XRF and XRD results. The new band at 1,362 cm^{-1} may correspond to NO_3^-. The observed NO_3^- vibration band indicated that there were positively charged iron species outside the interlayer of sepiolite. For this reason, the NO_3^- anions act as counter ions to balance the positive charge of the iron species [13]. The OH translation band at 784 cm^{-1} also disappeared. The shifts in the 477 and 430 cm^{-1} peaks for RS to 490 and 441 cm^{-1} for IOCS sample confirmed the involvement of the Si–O bond linkage in the modification. The Si–O stretching band at 980 cm^{-1} became sharp and shifted to 982 cm^{-1} after modification, which can be ascribed to the presence of Si–O–Fe bond [13,26]. The new absorption bands at 568 and 535 cm^{-1} revealed the existence of a new iron oxide phase on the sepiolite surface [13,27].

The FTIR results showed the existence of several functional groups including –OH and Si–OH, which are effective in the Cd(II) adsorption on IOCS (Fig. 4(c)). The shift in the

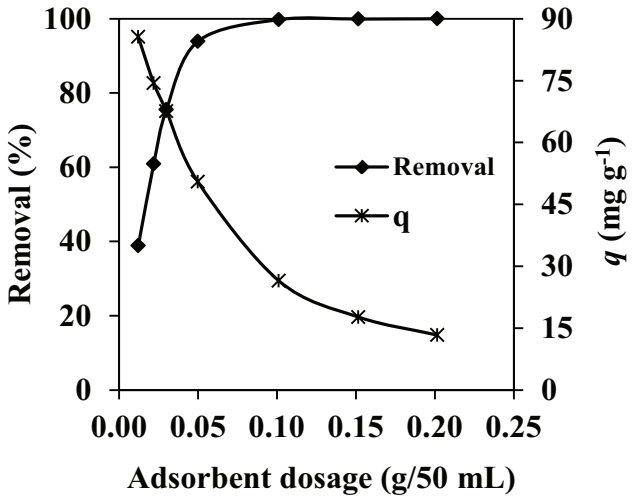

Fig. 4. Effect of adsorbent dosage on the removal of Cd(II) ions by IOCS (pH 6, contact time: 24 h, initial Cd(II) concentration: 50 mg L^{-1}, temperature: 25°C).

Table 3
Functional groups in RS, IOCS and IOCS-Cd samples

Functional group	Wavenumber (cm^{-1})		
	RS	IOCS	IOCS-Cd
Mg-OH stretching	3,691	3,690	3,690
–OH stretching	3,571–3,387–3,245	3,567–3,406–3,248	3,567–3,438–3,250
Carbonate impurity	2,534–1,820	–	–
–OH bending	1,654	1,635	1,635
Carbonate impurity	1,498–1,482	1,509	1,508
NO_3 vibration	–	1,362	1,385
Si–O stretching	1,209–1,078–980	1,210–1,078–982	1,209–1,078–982
Carbonate impurity	888	–	–
–OH bending	784	–	–
Si–O vibration	750	–	–
Carbonate impurity	730	–	–
Mg–OH bending	690–644	691–648	691–648
Fe–O vibration	593	590–568–535	598–560–538
O–Si–O bending	477	490	468
Si–O–Mg vibration	430	441	443

490 cm^{-1} band for IOCS sample to 468 cm^{-1} for IOCS-Cd sample confirms the involvement of the Si–O bond linkage in the Cd(II) adsorption process. After Cd(II) adsorption, a shift in the –OH stretching band from 3,406 to 3,438 cm^{-1} can be attributed to the attachment of Cd(II) on –OH group. A shift from 1,362 to 1,385 cm^{-1} was also observed after adsorption. This pointed out the interaction between Cd(II) and nitrate ions during adsorption. Further, the peaks attributing to Fe–O vibrations were shifted from 590, 568 and 535 cm^{-1} to 598, 560 and 538 cm^{-1}. These shifts indicated the involvement of iron nanoparticles in the adsorption of Cd(II) ions.

The oxygen atoms in the tetrahedral sheet, water molecules coordinated with the Mg^{2+} ions at the edge of the structure, and silanol groups caused by the break-up of Si–O–Si bonds are active adsorption centers on the sepiolite surfaces [28]. From the FTIR results, it may be concluded that the hydroxyl groups were believed to be involved in the Cd^{2+} adsorption on sepiolite surfaces. The shift in O–Si-O bending vibration further confirmed the formation of metal–silicate precipitates such as $CdSiO_3$ or Cd_2SiO_4 [29]. The most important finding from the FTIR results was the shifts in Fe–O vibration signals which confirmed the involvement of the iron oxide nanoparticles in the cadmium removal. The possible adsorption on IOCS may be due to physical adsorption, complexation with functional groups, surface precipitation or chemical reaction with surface. The changes in the FTIR spectra confirm the complexation of Cd(II) with functional groups present on the adsorbent sites [27].

3.2. Effect of adsorbent dosage

Different adsorbent dosages ranging from 0.01 to 0.20 g/50 mL were applied to investigate the effect of adsorbent dosage. Fig. 4 presents the results of the experiments. It is observed that the amount of Cd(II) adsorbed per unit mass of adsorbent (q) decreases with increase in the adsorbent dosage while the percentage removal of Cd(II) on IOCS increases rapidly up to 0.05 g/50 mL and becomes almost constant thereafter. This may be because of the increase in the surface area with increase in the adsorbent dosage. Further increment of adsorbent dosage was not so effective due to limited availability of the adsorbate around the adsorbent. A 93.93% Cd(II) removal was obtained at 0.05 g/50 mL adsorbent dosage. Furthermore, when the adsorbent dosage increased, the unsaturation of active sites on the surface occurred and therefore the adsorption capacity decreased [8].

3.3. Effect of pH

To study the adsorption capacity of the adsorbents, the initial pH value of the solution is an important factor. Therefore, optimization of the pH value is required. To better understand the effect of solution pH on the adsorption performance of IOCS, the investigation was carried out in the pH range of 2–6. This pH range was chosen to eliminate the formation of soluble hydroxyl complexes or precipitates based on the reason that Cd^{2+} started to precipitate when the pH was higher than 8 [30,31]. The results in Fig. 5 show that the adsorption decreases at lower pH and increases at high pH values. At lower pH values, the IOCS surface would be surrounded by hydrogen ions resulting in an increased competition of adsorption sites with metal ions. Increasing the pH of the solution leads to a decrease in the competition of hydrogen ions with metal ions for adsorption sites, and thus favouring higher removal of metal ions in the solution. The pH 6.0 was selected as the optimum pH value and employed in all the further experiments. Similarly, the cadmium removal by iron oxide modified adsorbents was reported to increase with increasing pH value [8,32]. The optimum pH for cadmium uptake was reported in the range from 5 to 7 in the previous studies [8,33].

3.4. Effect of contact time

The time required to reach equilibrium for the metal ions and adsorbent is of great importance in the adsorption experiment because it depends on the nature of the system used. The effect of contact time for the adsorption of cadmium onto IOCS at three different temperatures is presented in Fig. 6. The results indicated that the amount of cadmium adsorbed on IOCS increased with increasing contact time up

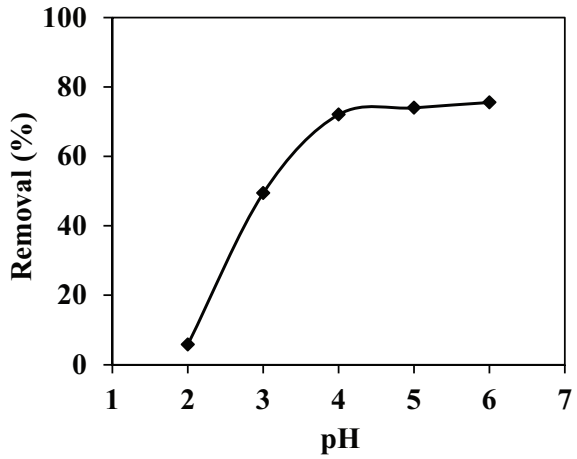

Fig. 5. Effect of pH on the removal of Cd(II) ions by IOCS (adsorbent dosage: 0.03 g/50 mL, contact time: 24 h, initial Cd(II) concentration: 50 mg L^{-1}, temperature: 25°C).

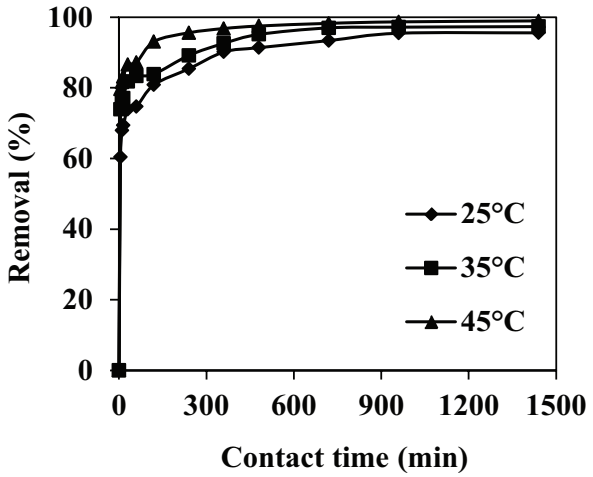

Fig. 6. Effect of contact time on the removal of Cd(II) ions by IOCS (adsorbent dosage: 0.05 g/50 mL, pH 6, initial Cd(II) concentration: 50 mg L^{-1}).

to 480 min, after which no further significant adsorption was recognized. Thus, it may be stated that the equilibrium was reached at about 8 h contacting period. The adsorption of cadmium ions seems to follow the two-phase sorption mechanism. The initial fast phase, especially in the first 5 min, occurs due to a larger surface area of the adsorbent being available for the adsorption of the metal ions. The subsequent slow phase occurs due to quick exhaustion of the adsorption sites. Similar results have been reported by other investigators for Cu(II) and Ni(II) adsorption onto iron-modified sepiolite samples [13,14]. It can also be observed from Fig. 6 that the Cd(II) adsorption slightly increases with an increase in the temperature from 25°C to 45°C. This situation indicated that the adsorption process was endothermic [13].

3.5. Effect of initial concentration

The equilibrium cadmium adsorption capacities of IOCS at various initial cadmium concentrations are depicted in Fig. 7. Cadmium adsorption was studied using different initial concentrations of 50, 100, 150, 200, 250, 300 and 500 mg L^{-1}, at 25°C, 35°C and 45°C temperatures. The adsorption capacity of cadmium (q_e) by IOCS in terms of mg of cadmium per gram of adsorbent increases with increasing concentration of cadmium as seen in Fig. 7. The cadmium adsorption capacity of IOCS increased from 50.44 to 97.08 mg g^{-1} as the initial concentration was varied from 50 to 500 mg L^{-1} at 25°C. The observed trend may be due to the increase in adsorption sites as a result of increase in metal concentrations. Higher metal concentration increases the affinity of Cd(II) ions to bind with the adsorbent [34]. It can also be seen from Fig. 7 that the adsorption capacity of IOCS increased with increasing temperature indicating the endothermic nature of the adsorption process [12,13].

3.6. Adsorption kinetics

In order to investigate the controlling mechanism of the adsorption processes, pseudo-first-order, pseudo-second-order and intraparticle diffusion kinetic models were applied to the experimental data. The pseudo-first-order equation can be expressed as follows [35]:

$$\log(q_e - q_t) = \log q_e - \frac{k_1 t}{2.303} \tag{3}$$

where k_1 (min^{-1}) is the rate constant of pseudo-first-order adsorption, q_e (mg g^{-1}) and q_t (mg g^{-1}) are the amounts of metal ion adsorbed per gram of IOCS at equilibrium and at any time t (min), respectively. A straight line for the plot of $\log(q_e - q_t)$ vs. t would give the first-order rate constant k_1 and equilibrium adsorption capacity q_e, from the slope and intercept of the line (Fig. 8(a)).

The pseudo-second-order kinetic rate equation can be given as [36] follows:

$$\frac{t}{q_t} = \frac{1}{k_2 q_e^2} + \frac{t}{q_e} \tag{4}$$

where k_2 (g mg^{-1} min^{-1}) is the rate constant of pseudo-second-order adsorption. The plot of t/q_t vs. t would give the pseudo-second-order rate constant k_2 and q_e (Fig. 8(b)).

The intraparticle diffusion model can be given as [37] follows:

$$q_t = k_p t^{1/2} \tag{5}$$

where k_p (mg g^{-1} $min^{-1/2}$) is the intraparticle diffusion rate constant. According to this model, the plot of q_t vs. $t^{1/2}$ (Fig. 8(c)) should be linear if intraparticle diffusion is involved in the adsorption process and if this line passes through the origin then intraparticle diffusion will be the rate controlling step. When the plot does not pass through the origin, this is indicative of some degree of boundary layer control and shows that the intraparticle diffusion is not the only rate limiting step, and other kinetic models may also control the rate of adsorption, all of which may be operating simultaneously.

Table 4 lists the kinetic parameters of pseudo-first-order, pseudo-second-order and intraparticle diffusion models. The correlation coefficients (R^2) for the pseudo-second-order kinetic model are higher than those for pseudo-first-order and intraparticle diffusion models, indicating that the pseudo-second-order model is more suitable for describing the adsorption behaviour of Cd(II) onto IOCS. Besides, the calculated q_e values by pseudo-second-order model were closer to the experimental q_{exp} than that of pseudo-first-order, suggesting that the curve modelled by pseudo-second-order model would be more consistent with the experimental data. As seen in Fig. 8(c), the plot did not pass through the origin and this deviation from the origin might be due to the difference in the mass transfer rate in the initial and final stages of adsorption. The adsorption of Cd(II) ions onto IOCS may be followed by an intraparticle diffusion model up to 5 min. This indicates that although intraparticle diffusion was involved in the adsorption process, it was not the only rate controlling step.

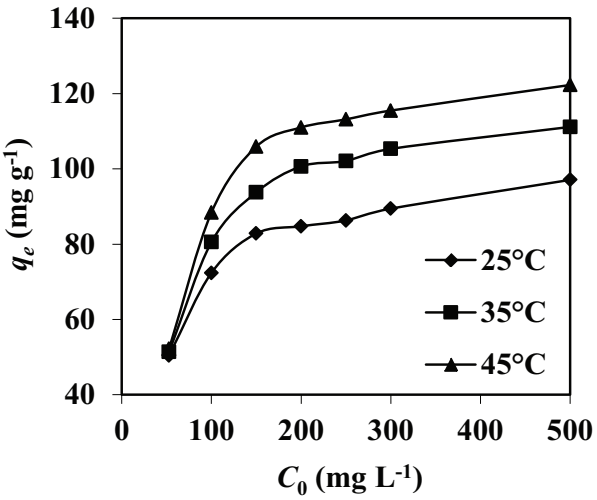

Fig. 7. Effect of initial concentration on the removal of Cd(II) ions by IOCS (adsorbent dosage: 0.05 g/50 mL, pH 6, contact time 24 h).

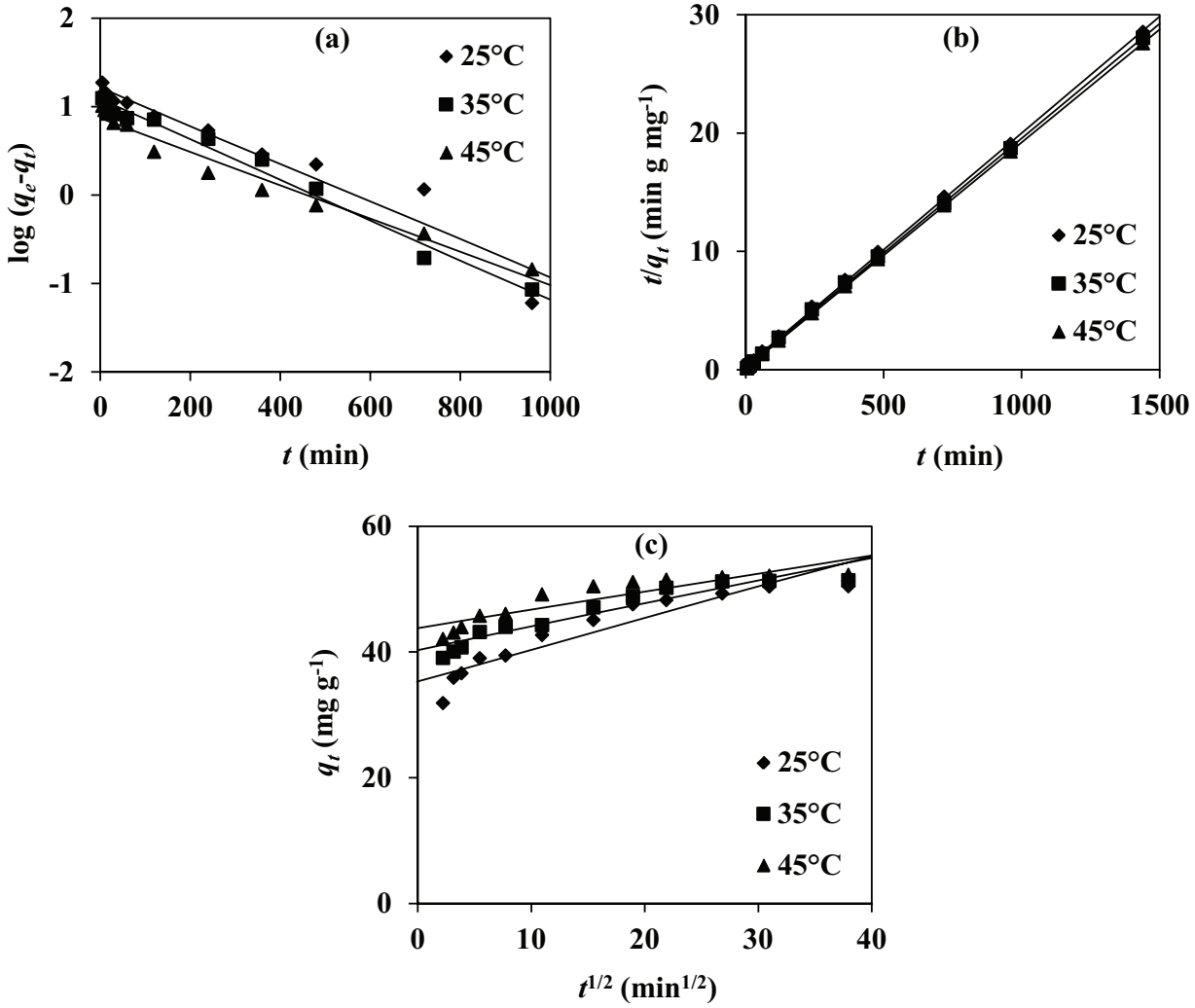

Fig. 8. Pseudo-first-order (a), pseudo-second-order (b) and intraparticle diffusion (c) plots for the adsorption of Cd(II) ions by IOCS.

Table 4
Kinetic parameters for the adsorption of Cd(II) ions by IOCS at different temperatures

T (°C)	q_{exp} (mg g^{-1})	Pseudo-first-order			Pseudo-second-order			Intraparticle diffusion	
		q_e (mg g^{-1})	k_1, 10^{-3} (min^{-1})	R^2	q_e (mg g^{-1})	k_2, 10^{-3} (g mg^{-1} min^{-1})	R^2	k_p, 10^{-3} (mg g^{-1} min$^{-1/2}$)	R^2
25	50.44	16.50	5.07	0.934	50.76	1.34	1.000	497.8	0.871
35	51.37	12.14	5.30	0.986	51.55	1.87	1.000	368.4	0.893
45	52.22	7.41	4.38	0.967	52.36	3.40	1.000	290.1	0.810

3.7. Adsorption isotherms

In order to identify the mechanism of the adsorption process, the adsorption isotherms are one of the most important data. Different isotherm models are available, among them more simple and reliable models Langmuir and Freundlich were used in the present study.

The Langmuir model assumes that the adsorbent surface is homogeneous and contains only one type of binding site so the energy of adsorption is constant, which can be expressed in linear form as [38] follows:

$$\frac{c_e}{q_e} = \frac{1}{bq_m} + \frac{c_e}{q_m} \tag{6}$$

where C_e (mg L^{-1}) is the equilibrium metal concentration in the solution, q_e (mg g^{-1}) is the amount of metal adsorbed per unit mass of adsorbent at equilibrium, b (L mg^{-1}) is the Langmuir constant related to the free adsorption energy, and q_m (mg g^{-1}) is the maximum adsorption capacity. The values of b and q_m can be determined from the intercept and the slope of the linear plot between C_e/q_e and C_e (Fig. 9(a)).

In order to predict whether an adsorption system is "favourable" or "unfavourable" the influences of isotherm shapes are widely used. One of the main features of the Langmuir isotherm can be described by means of R_L, a dimensionless constant referred to as separation factor or equilibrium parameter. R_L can be calculated using the following equation [39,40]:

$$R_L = \frac{1}{1 + bC_o} \tag{7}$$

where b is Langmuir constant and C_0 (mg L^{-1}) is the initial concentration of metal ions. The R_L parameter is considered as a more reliable indicator of the adsorption. There are four probabilities for the R_L value: for favourable adsorption $0 < R_L < 1$, for unfavourable adsorption $R_L > 1$, for linear adsorption $R_L = 1$ and for irreversible adsorption $R_L = 0$.

The Freundlich isotherm is an empirical model that proposes a monolayer sorption with heterogeneous energetic distribution of active sites. The linear form is given by [41]:

$$\log q_e = \log K_f + \frac{1}{n}\log C_e \tag{8}$$

where K_f (L g^{-1}) is roughly an indicator of the adsorption capacity and n of the adsorption intensity. The values of K_f and n can be determined from the linear plot of log q_e vs. log C_e (Fig. 9(b)). The obtained values of $n > 1$ signify favourable adsorption conditions.

Table 5 summarizes the values of various constants of these models and correlation coefficients calculated by the two models. As seen in Table 5, the correlation coefficients in Langmuir and Freundlich models were consistently higher than 0.95, meanwhile the correlation coefficients of Langmuir model were much nearer to 1.0. The results revealed that the Langmuir model proposed more satisfactory description on the Cd(II) adsorption onto IOCS, and further indicated the homogeneous surface of the adsorbent and the monolayer coverage of Cd(II) ions.

In the isotherm experiments, the calculated R_L values given in Table 5 are all within the range of $0 < R_L < 1$, revealing that the Cd(II) adsorption on IOCS was favourable. The calculated values of the Freundlich adsorption isotherm constant n were above unity, which also led to the conclusion that the adsorption process was favourable.

As seen from Table 5, the maximum adsorption capacity value of Cd(II) ions with IOCS, estimated from Langmuir model, was 98.04 mg g^{-1} at 25°C. This value was reported as 37.59 mg g^{-1} for RS in another study in which the same sepiolite was used [42]. This means that iron oxide coating increases cadmium adsorption capacity of sepiolite almost three times.

The maximum adsorption capacities of some adsorbents and IOCS for the removal of Cd(II) ions are given in Table 6. The experimental data of the present study are comparable with the reported values. The IOCS composite used in this study shows a high adsorption capacity compared with raw sepiolite and other adsorbents. The possible reasons are the porous structure and higher surface area of the adsorbent, and the affinity of iron oxide nanoparticles attached to the

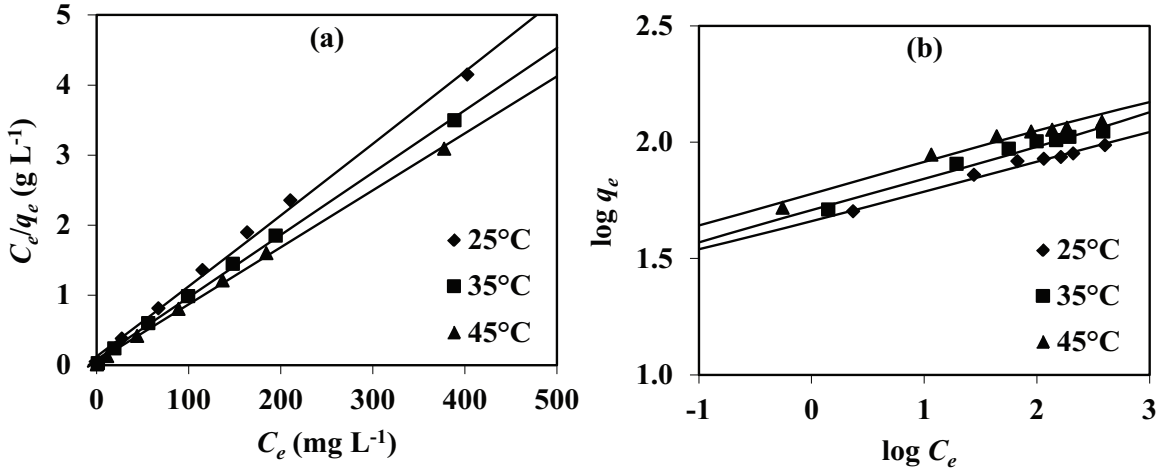

Fig. 9. Langmuir (a) and Freundlich (b) plots for the adsorption of Cd(II) ions by IOCS.

Table 5
Langmuir and Freundlich constants for the adsorption of Cd(II) ions by IOCS at different temperatures

T (°C)	Langmuir				Freundlich		
	q_m (mg g^{-1})	b, 10^{-2} (L mg^{-1})	R^2	R_L	K_f (L g^{-1})	n	R^2
25	98.04	7.97	0.997	0.02–0.20	46.54	7.98	0.983
35	112.36	10.88	0.999	0.02–0.16	51.09	7.15	0.977
45	123.46	14.73	0.999	0.01–0.12	59.94	7.62	0.963

Table 6
Comparisons of the Langmuir adsorption capacities (q_m) for Cd(II) adsorption by different adsorbents

Adsorbent	q_m (mg g^{-1})	T (°C)	pH	Refs.
Raw sepiolite (RS)	37.59	25	6	[42]
Iron oxide coated sepiolite (IOCS)	98.04	25	6	Present study
Iron oxide coated sewage sludge	14.70	25	5	[8]
Na-zeolitic tuff	17.63	30	6.2	[43]
Natural phosphate	29.41	Room temperature	5	[44]
Pen shells	37.63	25	4	[45]
Iron oxide modified clay-activated carbon composite	41.30	25	4.5	[32]
Heat-treated palygorskite	51.07	30	8.5	[46]
Grafted copolymer	51.55	25	6	[47]
Bentonite	63.29	–	5	[33]
Activated carbon	75.61	20	6	[48]
γ-Al_2O_3 nanoparticles	78.12	Room temperature	5	[49]
Alkali modified sewage sludge	80.15	25	5	[50]
Quartz sand-bentonite mixture	116.28	–	5	[33]

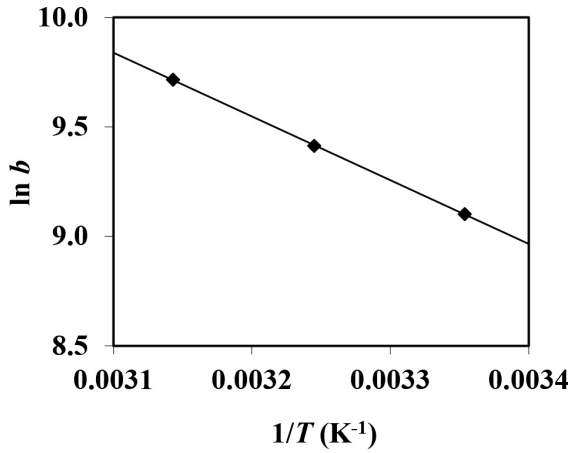

Fig. 10. Plot of ln b vs. 1/T for the estimation of thermodynamic parameters.

sepiolite surface for cadmium ion. By the way, the low cost of its residual support material and high adsorptive capacity make IOCS an economic and appealing adsorbent.

3.8. Thermodynamic parameters

Determination of thermodynamic parameters has a great importance to evaluate the spontaneity and the heat change of the adsorption processes. To estimate the effect of temperature on the adsorption of Cd(II) onto IOCS, the free energy change ($\Delta G°$), enthalpy change ($\Delta H°$), and entropy change ($\Delta S°$) values were determined. The relationship between the adsorption equilibrium constant (b) and temperature can be expressed by van't Hoff equation:

$$\ln b = \frac{-\Delta G°}{RT} = \frac{\Delta S°}{R} - \frac{\Delta H°}{RT} \quad (9)$$

where R is the universal gas constant (8.314 J mol^{-1} K^{-1}) and T is the absolute solution temperature (K). The values of $\Delta S°$ and $\Delta H°$ were calculated from the intercept and the slope of the linear plot of ln$b$ vs. 1/T (Fig. 10). From the values of $\Delta H°$ and $\Delta S°$, $\Delta G°$ can be calculated using the following relation:

Table 7
Thermodynamic parameters for the adsorption of Cd(II) ions by IOCS

$\Delta H°$	$\Delta S°$	$\Delta G°$ (kJ mol^{-1})		
(kJ mol^{-1})	(J mol^{-1} K^{-1})	25°C	35°C	45°C
24.18	156.76	–22.56	–24.11	–25.70

$$\Delta G° = \Delta H° - T\Delta S° \quad (10)$$

The calculated parameters are given in Table 7. The negative values of $\Delta G°$ at all the temperatures indicated that the Cd(II) adsorption on IOCS was spontaneous and thermodynamically feasible. The positive values of $\Delta H°$ suggested that the adsorption of Cd(II) on IOCS was endothermic in nature and consequently increased the adsorption capability with the increase in temperature. This is in agreement with the decrease in $\Delta G°$ with increasing temperature. The positive values of $\Delta S°$ indicated a decrease in the order of the system.

4. Conclusions

The present study proves the capability and effectiveness of IOCS as an adsorbent for cadmium removal. The successful coating of iron oxide onto sepiolite was evidenced via the results obtained using the XRD, XRF, BET, SEM, EDS and FTIR techniques. The adsorption behaviour of Cd(II) was affected by experimental parameters such as adsorbent dosage, pH, contact time, initial concentration and temperature. The adsorption process could be described well by the pseudo-second-order kinetic model and the Langmuir isotherm model. The maximum adsorption capacity of Cd(II) ions by IOCS, estimated from Langmuir model, was 98.04 mg g^{-1} at 25°C. The estimated values of $\Delta H°$ (24.18 kJ mol^{-1}) and $\Delta S°$ (156.76 J mol^{-1} K^{-1})

indicated the endothermic nature of adsorption and enhanced the randomness at the adsorbent–adsorbate interface. The negative $\Delta G°$ values (–22.56 to –25.70 kJ mol^{-1} for 25°C–45°C) confirmed the spontaneous nature of the adsorption. The results obtained in this study show that IOCS is an effective adsorbent for the removal of cadmium and can be used in water and wastewater treatments.

References

[1] Y. Huang, S. Li, J. Chen, X. Zhang, Y. Chen, Adsorption of Pb(II) on mesoporous activated carbons fabricated from water hyacinth using H_3PO_4 activation: adsorption capacity, kinetic and isotherm studies, Appl. Surf. Sci., 293 (2014) 160–168.

[2] E.N. Zare, A. Motahari, M. Sillanpaa, Nanoadsorbents based on conducting polymer nanocomposites with main focus on polyaniline and its derivatives for removal of heavy metal ions/dyes: a review, Environ. Res., 162 (2018) 173–195.

[3] C.-Y. Cao, C.-H. Liang, Y. Yin, L.-Y. Du, Thermal activation of serpentine for adsorption of cadmium, J. Hazard. Mater., 329 (2017) 222–229.

[4] WHO, Guidelines for Drinking-Water Quality, 4th edition, WHO, Switzerland, 2011.

[5] T.C. Nguyen, P. Loganathan, T.V. Nguyen, S. Vigneswaran, J. Kandasamy, R. Naidu, Simultaneous adsorption of Cd, Cr, Cu, Pb, and Zn by an iron-coated Australian zeolite in batch and fixed-bed column studies, Chem. Eng. J., 270 (2015) 393–404.

[6] N.P. Raval, P.U. Shah, N.K. Shah, Adsorptive removal of nickel(II) ions from aqueous environment: a review, J. Environ. Manage., 179 (2016) 1–20.

[7] M.-D. Ma, H. Wua, Z.-Y. Deng, X. Zhao, Arsenic removal from water by nanometer iron oxide coated single-wall carbon nanotubes, J. Mol. Liq., 259 (2018) 369–375.

[8] T. Phuengprasop, J. Sittiwong, F. Unob, Removal of heavy metal ions by iron oxide coated sewage sludge, J. Hazard. Mater., 186 (2011) 502–507.

[9] M. Alkan, G. Tekin, H. Namli, FTIR and zeta potential measurements of sepiolite treated with some organosilanes, Microporous Mesoporous Mater., 84 (2005) 75–83.

[10] M. Mora, M.I. Lopez, M.A. Carmona, C. Jimenez-Sanchidrian, J.R. Ruiz, Study of the thermal decomposition of a sepiolite by mid- and near-infrared spectroscopies, Polyhedron, 29 (2010) 3046–3051.

[11] Y. Zhang, L. Wang, F. Wang, J. Liang, S. Ran, J. Sun, Phase transformation and morphology evolution of sepiolite fibers during thermal treatment, Appl. Clay Sci., 143 (2017) 205–211.

[12] E. Eren, H. Gumus, Characterization of the structural properties and Pb(II) adsorption behavior of iron oxide coated sepiolite, Desalination, 273 (2011) 276–284.

[13] E. Eren, H. Gumus, N. Ozbay, Equilibrium and thermodynamic studies of Cu(II) removal by iron oxide modified sepiolite, Desalination, 262 (2010) 43–49.

[14] S. Lazarevic, I. Jankovic-Castvan, V. Djokic, Z. Radovanovic, D. Janackovic, R. Petrovic, Iron-modified sepiolite for Ni^{2+} sorption from aqueous solution: an equilibrium, kinetic, and thermodynamic study, J. Chem. Eng. Data, 55 (2010) 5681–5689.

[15] Z. Orolinova, A. Mockovciakova, Structural study of bentonite/iron oxide composites, Mater. Chem. Phys., 114 (2009) 956–961.

[16] Z. Lu, Z. Hao, J. Wang, L. Chen, Efficient removal of europium from aqueous solutions using attapulgite-iron oxide magnetic composites, J. Ind. Eng. Chem., 34 (2016) 374–381.

[17] R.L. Frost, O.B. Locos, H. Ruan, J.T. Kloprogge, Near-infrared and mid-infrared spectroscopic study of sepiolites and paligorskites, Vib. Spectrosc., 27 (2001) 1–13.

[18] F. Franco, M. Pozo, J.A. Cecilia, M. Benítez-Guerrero, E. Pozo, J.A. Martín Rubí, Microwave assisted acid treatment of sepiolite: the role of composition and "crystallinity", Appl. Clay Sci., 102 (2014) 15–27.

[19] L. Lescano, L. Castillo, S. Marfil, S. Barbosa, P. Maiza, Alternative methodologies for sepiolite defibering, Appl. Clay Sci., 95 (2014) 378–382.

[20] İ. Kıpçak, T.G. Isıyel, Magnesite tailing as low-cost adsorbent for the removal of copper (II) ions from aqueous solution, Korean J. Chem. Eng., 32 (2015) 1634–1641.

[21] E. Sabah, S. Ouki, Sepiolite and sepiolite-bound humic acid interactions in alkaline media and the mechanism of the formation of sepiolite-humic acid complexes, Int. J. Miner. Process., 162 (2017) 69–80.

[22] X. Wu, Q. Zhang, C. Liu, X. Zhang, D.D.L. Chung, Carbon-coated sepiolite clay fibers with acid pre-treatment as low cost organic adsorbents, Carbon, 123 (2017) 259–272.

[23] Y. Qiu, S. Yu, Y. Song, Q. Wang, S. Zhong, W. Tian, Investigation of solution chemistry effects on sorption behavior of Sr(II) on sepiolite fibers, J. Mol. Liq., 180 (2013) 244–251.

[24] A.A. Ahribesh, S. Lazarevic, I. Jankovic-Castvan, B. Jokic, V. Spasojevic, T. Radetic, D. Janackovic, R. Petrovic, Influence of the synthesis parameters on the properties of the sepiolite-based magnetic adsorbents, Powder Technol., 305 (2017) 260–269.

[25] O. Duman, S. Tunç, T.G. Polat, Adsorptive removal of triarylmethane dye (Basic Red 9) from aqueous solution by sepiolite as effective and low-cost adsorbent, Microporous Mesoporous Mater., 210 (2015) 176–184.

[26] Z. Xu, H. Jiang, Y. Yu, J. Xu, J. Liang, L. Zhou, F. Hu, Activation and β-FeOOH modification of sepiolite in one-step hydrothermal reaction and its simulated solar light catalytic reduction of Cr(VI), Appl. Clay Sci., 135 (2017) 547–553.

[27] M. Jain, M. Yadav, T. Kohout, M. Lahtinen, V.K. Garg, M. Sillanpaa, Development of iron oxide/activated carbon nanoparticle composite for the removal of Cr(VI), Cu(II) and Cd(II) ions from aqueous solution, Water Resour. Ind., 20 (2018) 54–74.

[28] A. Yebra-Rodriguez, J.D. Martin-Ramos, F. Del Rey, C. Viseras, A. Lopez-Galindo, Effect of acid treatment on the structure of sepiolite, Clay Miner., 38 (2003) 353–360.

[29] L.-Y. Gao, J.-H. Deng, G.-F. Huang, K. Li, K.-Z. Cai, Y. Liu, F. Huang, Relative distribution of Cd^{2+} adsorption mechanisms on biochars derived from rice straw and sewage sludge, Bioresour. Technol., 272 (2019) 114–122.

[30] N. Balkaya, H. Cesur, Adsorption of cadmium from aqueous solution by phosphogypsum, Chem. Eng. J., 140 (2008) 247–254.

[31] Y. Feng, J.L. Gong, G.M. Zeng, Q.Y. Niu, H.Y. Zhang, C.G. Niu, J.H. Deng, M. Yan, Adsorption of Cd (II) and Zn (II) from aqueous solutions using magnetic hydroxyapatite nanoparticles as adsorbents, Chem. Eng. J., 162 (2010) 487–494.

[32] R.R. Pawar, Lalhmunsiama, M. Kim, J.-G. Kim, S.-M. Hong, S.Y. Sawant, S.M. Lee, Efficient removal of hazardous lead, cadmium, and arsenic from aqueous environment by iron oxide modified clay-activated carbon composite beads, Appl. Clay Sci., 162 (2018) 339–350.

[33] T. Schütz, S. Dolinska, P. Hudec, A. Mockovciakova, I. Znamenackova, Cadmium adsorption on manganese modified bentonite and bentonite–quartz sand blend, Int. J. Miner. Process., 150 (2016) 32–38.

[34] S.R. Mishra, R. Chandra, J. Kaila, S. Darshi, Kinetics and isotherm studies for the adsorption of metal ions onto two soil types, Environ. Technol. Innovation, 7 (2017) 87–101.

[35] S. Lagergren, Zur theorie der sogenannten adsorption gelöster stoffe, K. Sven. Vetensk.akad. Handl., 24 (1898) 1–39.

[36] Y.S. Ho, G. McKay, Sorption of dye from aqueous solution by peat, Chem. Eng. J., 70 (1998) 115–124.

[37] W.J. Weber, J.C. Morris, Kinetics of adsorption on carbon from solution, J. Sanitary Eng. Div. ASCE, 89 (1963) 31–59.

[38] I. Langmuir, The adsorption of gases on plane surfaces of glass, mica and platinum, J. Am. Chem. Soc., 40 (1918) 1361–1403.

[39] K.R. Hall, L.C. Eagleton, A. Acrivos, T. Vermeulen, Pore- and solid diffusion kinetics in fixed-bed adsorption under constant-pattern conditions, Ind. Eng. Chem. Fundam., 5 (1966) 212–223.

[40] T.W. Weber, R.K. Chakravorti, Pore and solid diffusion models for fixed bed adsorbers, J. Am. Inst. Chem. Eng., 20 (1974) 228–238.

[41] H. Freundlich, Colloid and Capillary Chemistry, Methuen, London, 1926.

[42] İ. Kıpçak, S. Erol, C. Gürakan, Removal of Cd(II) Ions from Aqueous Solution by Sepiolite (in Turkish), 11th National

Chemical Engineering Congress, Book of Abstract, Eskişehir, Turkey, 2014, pp. 650–651.
[43] E. Gutierrez-Segura, M. Solache-Rios, A. Colin-Cruz, C. Fall, Adsorption of cadmium by Na and Fe modified zeolitic tuffs and carbonaceous material from pyrolyzed sewage sludge, J. Environ. Manage., 97 (2012) 6–13.
[44] H. Yaacoubi, O. Zidani, M. Mouflih, M. Gourai, S. Sebti, Removal of cadmium from water using natural phosphate as adsorbent, Procedia Eng., 83 (2014) 386–393.
[45] C. Jeon, Adsorption behavior of cadmium ions from aqueous solution using pen shells, J. Ind. Eng. Chem., 58 (2018) 57–63.
[46] W. Wang, H. Chen, A. Wang, Adsorption characteristics of Cd(II) from aqueous solution onto activated palygorskite, Sep. Purif. Technol., 55 (2007) 157–164.
[47] P.U. Shah, N.P. Raval, N.K. Shah, Cadmium(II) removal from an aqueous solution using CSCMQ grafted copolymer, Desal. Wat. Treat., 57 (2016) 28262–28273.
[48] F. Sardella, M. Gimenez, C. Navas, C. Morandi, C. Deiana, K. Sapag, Conversion of viticultural industry wastes into activated carbons for removal of lead and cadmium, J. Environ. Chem. Eng., 3 (2015) 253–260.
[49] S. Tabesh, F. Davar, M.R. Loghman-Estarki, Preparation of γ-Al_2O_3 nanoparticles using modified sol-gel method and its use for the adsorption of lead and cadmium ions, J. Alloys. Compd., 730 (2018) 441–449.
[50] J.-L. Hu, X.-W. He, C.-R. Wang, J.-W. Li, C.-H. Zhang, Cadmium adsorption characteristic of alkali modified sewage sludge, Bioresour. Technol., 121 (2012) 25–30.